ELSEVIER

Journal of Nuclear Materials 280 (2000) 73–85

journal of nuclear materials

www.elsevier.nl/locate/jnucmat

Influence of the interatomic potentials on molecular dynamics simulations of displacement cascades

C.S. Becquart [a,*], C. Domain [b], A. Legris [a], J.C. Van Duysen [a,b]

[a] *Laboratoire de Métallurgie Physique et Génie des Matériaux, UMR 8517, Bât. C6, Université Lille I, F-59655 Villeneuve d'Ascq Cedex, France*

[b] *EDF – DER Département EMA, Les renardières, F-77818, Moret sur Loing Cedex, France*

Received 10 August 1999; accepted 8 February 2000

Abstract

Molecular dynamics (MD) is a powerful tool to study the displacement cascades initiated by the neutrons when they interact with matter. Key components of this technique are the interatomic potentials which model the binding of the different constitutive atoms. There exist many interatomic potentials dedicated to α-Fe and we have tested three of them for the study of radiation damage. We have found that the primary damage is potential sensitive. From our study, it appears that some characteristics of the potentials, not always considered, can be correlated to the type of damage produced by displacement cascades. The repulsive part of the potential has a strong influence on the cascade morphology. Moreover, equilibrium properties such as the atoms mean square displacements, the vacancy migration and vacancy–vacancy binding energies also appear to have some influence and should be investigated carefully when simulating radiation damage. It is therefore very important to use extreme care when trying to obtain quantitative results from MD simulations.

PACS: 61.43.B; 61.80; 61.72

1. Introduction

Because of the length and time scales (nm and ps) involved in displacement cascades, molecular dynamics (MD) has been extensively used [1–7] to simulate radiation damage creation since the pioneering work of Gibson et al. [8]. Some recent developments among others concern the size of the system under study and nowadays it is possible to simulate millions of atoms if empirical interatomic potentials are employed for the cohesive model. In this kind of scheme, a functional form for the interatomic potential is assumed and the potential parameters are fitted to experimental and/or theoretical data. Inherent to the use of empirical potentials is the transferability which will determine the degree of confidence one may have in the results. In this case, transferability is the ability of a potential fitted mostly on equilibrium properties to model situation far from equilibrium such as displacement cascades.

Among the different materials under irradiation, one finds the pressure vessel steels of light water reactors. It is now well established that Cu plays an important role in the embrittlement induced by the neutrons in such materials, and we have thus undertaken a study to characterize the effects of irradiation in model Fe–Cu binary alloys by atomistic simulations. We performed MD simulations with different energies and different FeCu potentials for very dilute alloys (at.%Cu = 0.2).

The objective of this work is to compare the results obtained from the simulation of displacement cascades with different interatomic potentials in order to determine the influence of various properties on the estimation of the residual damage. This task is essential in

* Corresponding author.

E-mail addresses: charlotte.becquart@univ-lille1.fr (C.S. Becquart), christophe.domain@edf.fr (C. Domain), alexandre.legris@univ-lille1.fr (A. Legris), jean-claude.van-duysen@edf.fr (J.C. Van Duysen).

0022-3115/00/$ - see front matter
PII: S0022-3115(00)00029-5

order to predict quantitative and accurate information on radiation damage from MD simulations.

With this objective in mind, we compare, when possible, our results with those obtained by Calder et al. [3], Phythian et al. [9] Stoller et al. [10] and Gao et al [11]. All these groups worked with the same Fe interatomic potential, different from ours and later referred to as 'Finnis type' potential.

The article is organized as follows.

In a first part, we outline the computational procedure for displacement cascade simulations and the potentials used in this work. We then compare the basic properties of the potentials. As we have studied FeCu alloys with very low Cu contents, we will focus mostly on the interactions between Fe atoms and will briefly describe the FeCu components. In the result section we examine the damage obtained with the different potentials. For our purpose, the damage is characterized by the number of residual defects and their tendency to form clusters (number and size of the clusters). In the discussion section, we propose some explanations for the different behaviors observed in this work and correlate them when possible with characteristics of the potentials.

2. Methods

2.1. Interatomic potentials

The potentials used were built according to the embedded atom method (EAM) [12] for the simulations we performed, or within Finnis Sinclair's (FS) approach [13] for the Finnis type potential work. In addition to pair interactions, both potentials implement an extra energy (*embedding energy* for EAM, *bonding term* for FS) which approximates the many-body contribution of nearby atoms.

The total potential energy is then given by

$$E = \sum_{i<j=1}^{N} V_{ij}(r_{ij}) + \sum_{i=1} F_i(\rho_i),$$

where the value of ρ_i is given by

$$\rho_i = \sum_{j\neq i}^{N} \Phi_j(r_{ij}).$$

E is the total potential energy of all atoms i. It has two parts. The first term on the right side of the above equation is the pair potential term, the sum is over all neighboring atoms j of atom i. Variable r_{ij} is the distance between atom i and its neighbor j. The second part is the embedding energy, F_i is the embedding function, and ρ_i is the electron density around atom i, contributed by its neighbors.

All the potentials studied in this work have been published elsewhere and the precise forms for the different functions can be found in the original publications.

Fe I potential. Fe I is a potential derived by Harrison et al. [14], (potential labeled FEB in Ref. [14]). It was initially designed for interaction distances greater than 0.1 nm. To be suitable for simulations of cascades, it was hardened by Turbatte [15] following the procedure of Prönnecke et al. [16].

Fe II potential. Fe II is a potential derived by Haftel et al. [17] (potential labeled 4 in Ref. [17]). Its hardening is based on the work of Vascon [18,19].

Fe III potential. Fe III was derived by Simonelli et al. [20], it was suitably adjusted to the simulation of displacement cascades by Raulot [21].

Finnis type potential. this potential was originally derived by Finnis et al. [13] and adapted to the simulation of displacement cascades by Calder et al. [3].

All these potentials have been adjusted to reproduce some equilibrium and defect properties which are summarized in Tables 1–3.

2.2. Computational procedure

The MD was performed using DYMOKA [22], a parallelized and slightly modified version of CDCMD [23], a standard MD package that uses a fifth order Gear predictor–corrector algorithm. The defect energies were calculated using the energy minimization method algorithm called quench molecular dynamics (QMD) derived after [24,25].

As was previously mentioned, we are interested in simulating the effect of neutron irradiation. It is well known that neutrons produce displacement cascades which are initiated when an atom in the solid, the primary knocked-on atom (PKA) receives via an elastic collision an energy higher than a few hundred eV. The subsequent cascade development can be roughly divided into three phases: the collision phase, lasting $\sim 10^{-13}$ s, during which the PKA energy is shared among successive generations of recoil atoms, a relaxation period, which lasts less than a picosecond during which defects begin to assume their equilibrium configurations and a cooling phase which lasts a few picoseconds during which the highly disordered cascade volume reaches local thermal equilibrium with the surrounding lattice.

For the simulations, we used periodic boundary conditions (PBC). The choice of the simulation box size depends upon the energy of the PKA. It must be large enough to avoid the displacement cascade to interfere with itself by periodic overlap. The number of atoms in the bcc cubic crystal for each PKA ranges from about 20 000 for a 100 eV cascade up to 3 456 000 for a 30 keV one.

Table 1
Typical data fitted upon: equilibrium lattice constant, cohesive energy, elastic constants for α-Fe

	Fe I	Fe II	Fe III	Finnis type potential[a]	Experimental
a_0 (Å)	2.8669	2.8665	2.8664	2.8665	2.87[b]
E_{coh} (eV)	4.28	4.28	4.28	4.316	4.28[b]
C_{11} (10^{11} Pa)	2.12	2.33	2.42	2.433	2.43[c], 2.33[d], 2.37[e]
C_{12} (10^{11} Pa)	1.53	1.37	1.47	1.450	1.38[c], 1.35[d], 1.41[e]
C_{44} (10^{11} Pa)	1.15	1.18	1.12	1.16	1.22[c], 1.18[d], 1.16[e]
C' (10^{11} Pa)	0.29	0.48	0.48	0.492	0.53[c], 0.49[d], 0.48[e]

[a] Ref. [30]; [b] Ref. [26]; [c] Ref. [27]; [d] Ref. [28]; [e] Ref. [29].

Table 2
Vacancy formation and migration energies, relaxed vacancy–vacancy binding energy for α-Fe[a]

	Fe I	Fe II	Fe III	Finnis type potential	Experimental
E^f_{vac} (eV)	2.14	1.41	1.63	1.83	≈2[b], 1.53[c]
E^m_{vac} (eV)	0.101	1.45	0.66	0.91[d]	0.55[e]
Relaxed E_{VV} (eV)	0.48 (2nn)	0.41 (1nn)	0.21 (2nn)	0.19[f] (2nn)	–

[a] 1nn indicates that the divacancy is the most stable when the two vacancies are in first nearest neighbor positions, 2nn when they are in second nearest neighbor positions.
[b] Ref. [31]; [c] Ref. [32]; [d] Ref. [3]; [e] Ref. [33]; [f] Ref. [34].

Table 3
Self interstitial formation energies for α-Fe

	Fe I	Fe II	Fe III	Finnis type potential
Dumbbell ⟨1 1 1⟩	Becomes crowdion	Becomes crowdion	Becomes crowdion	4.87[a]
Dumbbell ⟨1 1 0⟩	2.95	6.98	3.67	4.76[a]
Dumbbell ⟨1 0 0⟩	6.04	10.03	4.57	–
Crowdion	2.59	6.77	3.54	4.91[a]

[a] Ref. [10].

At the beginning of the simulation, the system of particles is let to equilibrate, for 5 ps, at the chosen temperature, most of the time 600 K to be close to the vessel irradiation temperature. When the lattice is at thermal equilibrium, one atom, the PKA, is given a momentum corresponding to energies varying from 1 to 30 keV. The actual time step varies from 10^{-17} s (at the beginning of the collision phase) to 10^{-15} s in order to keep the total energy constant.

The following approximations were made:

- following many authors scheme [3,9], the electron–phonon couplings have not been taken into account;
- the boundary atoms were not damped to extract heat or attenuate the out-going pressure wave. According to Phythian et al. [9], the drift temperature dependence of the residual defects and the defect clustering fraction is weak. This has been confirmed by Gao et al. [11] who investigated the problem very thoroughly.

Our simulations were done in the microcanonical ensemble with PBC, while the simulations done by Calder et al. and Stoller et al. were done at constant pressure.

Variability was introduced by changing the initial distribution of the velocities, the random distribution of the Cu atoms (in solid solution) and also the PKA's direction.

The PKA directions, ⟨1 3 5⟩ and ⟨2 5 3⟩, were chosen to be representative of an average behavior. Stoller et al. [10] examined the influence of the PKA direction and their results support the view that the ⟨1 3 5⟩ cascades should provide a reasonable representation of average behavior. We have observed similar trends and all the results presented below were obtained either with ⟨1 3 5⟩ or ⟨2 5 3⟩.

To distinguish between the crystallographic point defects, different characterizations are possible. In this work, we used the scheme developed by Vascon [19]: it allows the identification of vacancies, true or single interstitials, dumbbells and replaced atoms.

The group using the Finnis type potential adopted a slightly different detection method that allows them to detect vacancies and interstitials without making a distinction between true interstitials and dumbbells. In what follows, and to be able to compare with the Finnis type potential results, we will not distinguish between

the different interstitial types: true interstitials or dumbbells. We have used this method to

- detect the number of residual defects at the end of the cascade;
- define the cascade peak as the configuration corresponding to the maximum count of point defects.

The methods described above may not be as precise as the construction of Wigner Seitz cells at each lattice site, but they are easier to implement and fast. In principle, they give the same results than the latter in respect of residual damage. They may differ however in the precise number of defects they count at the cascade peak. That is why we always compare the different potentials results without paying much attention to the actual number of defects at the peak.

The amount of incascade clustering is important since small defects clusters can be very mobile and provide easy nucleation sites for larger defects to grow. As di-vacancies tend to be in second nearest-neighbor position, we define a vacancy cluster as a configuration in which each vacancy has at least one second nearest-neighbor position occupied by a vacancy. For the interstitials, the two defects have to be within the nearest-neighbor distance to belong to the same cluster.

3. Comparison of the potentials

We present below the interatomic potentials relevant properties which could significantly influence the primary damage creation and its subsequent evolution, emphasizing on the Fe parts.

3.1. α-Fe

The three potentials we used were fitted to the usual experimental data: the cohesive energy, the elastic constants and the vacancy formation energy. As can be seen from Table 1, these data are reproduced correctly. One should note however that for Fe I, the errors on C_{11} and C_{12} add up and give a very low value of C'.

3.1.1. Defect energies

The point defects (vacancies and interstitials) formation energies are very sensitive data. The experimental values are quite widespread when they exist and the calculated ones are very much potential dependent.

3.1.1.1. Vacancies. The vacancy formation energy, E^{f}_{vac}, is generally fitted upon. It appears clearly that the vacancy formation energies of the potentials are quite different (Table 2), but the experimental data span is large too and most of the potentials fall inside the experimental range. We have also observed that the relaxation around the vacancy is quite important and gives rise to an important energy difference (for instance 0.12 eV for Fe III). This fact has been confirmed by ab initio calculations [35].

There has been some controversy about the experimental vacancy migration energy: for instance Schaefer et al. [32] found a value of 1.28 eV. This scattering is very likely due to the presence of a very small amount of impurity atoms which modify greatly the diffusion coefficient. Indeed the 0.55 eV value has been measured for a high purity α-Fe [33].

Given the short period of time involved in cascade damage generation, we do not expect this parameter to control the defects migration in the usual way (thermal diffusion). However, it may be seen as a measure of the roughness of the potential and in that sense it may influence the athermal migration of defects during the relaxation and cooling phases.

The vacancy binding energy is an important parameter for the formation of vacancy clusters and voids. Unfortunately, no experimental data is available to compare to. Masuda [36] investigated the properties of vacancy-type lattice defects in bcc transition metals using a tight binding type electronic theory. His results show that the most stable relaxed configuration for the divacancy in transition metals is when the vacancies are second nearest neighbors. This is also observed experimentally [37] in Mo and is indeed the case with three out of the four potentials as can be seen in Table 2. From these results, it obviously appears that the binding energies are quite different from one potential to another.

3.1.1.2. Interstitials. The values (see Table 3) obtained for Fe I, Fe II and Fe III were calculated by the QMD procedure. The two dumbbell atoms were forced to remain on a line running in the initial (⟨1 0 0⟩, ⟨1 1 0⟩ or ⟨1 1 1⟩) direction (constrained QMD) otherwise they spontaneously rotate to the ⟨1 1 1⟩ direction.

The most stable interstitial-type defect predicted by the three potentials studied in this work is an 'activated' crowdion along ⟨1 1 1⟩ (five Fe atoms sharing four lattice sites), while the most stable defect observed experimentally is a dumbbell along ⟨1 1 0⟩ [38,39]. This discrepancy is a common problem shared by many interatomic potentials for bcc Fe, the reason seems to be correlated with the range of the potential (its cut-off). Indeed, it seems that EAM-like potentials with ranges above the third nearest neighbor cannot stabilize the right kind of interstitial defects [20]. This fact has been also observed by Osetsky et al. [40] comparing simulations done with the short range Finnis type potential to simulations done with a long range pair potential. However, whatever the potential range, and therefore whatever the type of dumbbell stabilized, Osetsky et al.'s work [40] shows that it does not influence very much the dynamics of interstitial clusters.

Sensible differences can be observed between the potentials. That fact is worth noticing, as these energies

may have some influence in the cascade core interstitial defects formation. Unfortunately, to our knowledge, no experimental data is available for the self interstitial formation energies.

3.1.2. Stability of the bcc structure

Because of the high energy concentration in the cascade core during the collision phase, the bcc structure vanishes. To have a small insight on the ability of the potential to give realistic information of the cascade core structure, we investigated the stability of the bcc phase with respect to the fcc and hcp phases. The results are summarized in Table 4 along with some other published results. Because all but Osetsky's potentials are short ranged, the fcc–hcp energy difference is 0, which is not the case experimentally.

3.1.3. Thermal properties

The thermal dilation is representative of the anharmonicity of the potential. We have plotted, Fig. 1, the evolution of the lattice parameter for the three different potentials. Sensible differences can be observed among the potentials, potential Fe I gives a dilation coefficient closer to the experimental results.

The mean square displacement (MSD) characterizes the mean amplitude of the thermal vibration of the atoms around their site. We calculated it for the three potentials versus temperature. From Fig. 2, it appears that the MSD behavior for Fe III agrees very well with experimental measurements whereas the other two potentials, Fe I and Fe II, lay either too high or too low.

The melting temperatures were determined according to the Lindemann [44] criterion $\langle \mathrm{MSD}^2(T_{\mathrm{melting}})\rangle = \delta^2 d^2$, where d is the first nearest-neighbor distance and δ a parameter estimated to be 0.0767 for Fe [45]. With this criterion, Fe I (resp. Fe II, Fe III) melts around 1400 K (3850, 2200 K, respectively). The experimental melting temperature of pure Fe is 1811 K. We do not know the thermal behavior of the Finnis type potential, only that its melting temperature has been estimated to be 2200 ± 200 K [3]. Diffusion in the melt is an important parameter in determining the primary state of damage [1] and the differences observed in the thermal properties can be meaningful.

3.1.4. Cascade oriented properties

The threshold displacement energy is the minimum kinetic energy one must give an atom to create a stable Frenkel pair in the lattice. It depends on the materials and on the orientation of the primary recoil. The threshold displacement energies are the only parameters fitted to in the hardening procedure, they therefore are the only physical quantities giving insight on the short distance interactions. Table 5 presents the threshold displacement energies for the three high symmetry crystallographic directions for which experimental data are available [46]. In our calculations, we consider a Frenkel pair to be stable (notice that the calculations are done at 0 K) when the vacancy lasts at least 5 ps. The energies are quite

Table 4
Energy differences between the bcc, fcc and hcp phases

	Fe I	Fe II	Fe III	Finnis type potential	Fe Osetsky[a]	Ab initio calculations
$\Delta E_{\mathrm{bcc\text{-}fcc}}$ (eV)	0.056	0.032	0.027	0.054	0.056	0.035[b], 0.08[c]
$\Delta E_{\mathrm{bcc\text{-}hcp}}$ (eV)	0.056	0.032	0.027	0.054	0.073	0.12[b], 0.11[c]

[a] Ref. [41]; [b] Ref. [42]; [c] Ref. [43].

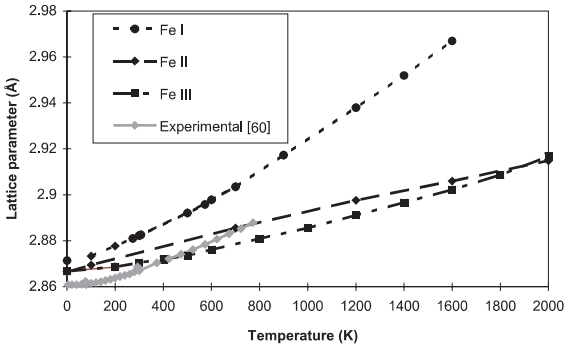

Fig. 1. Lattice parameter dilation with temperature for Fe I, Fe II and Fe III [60].

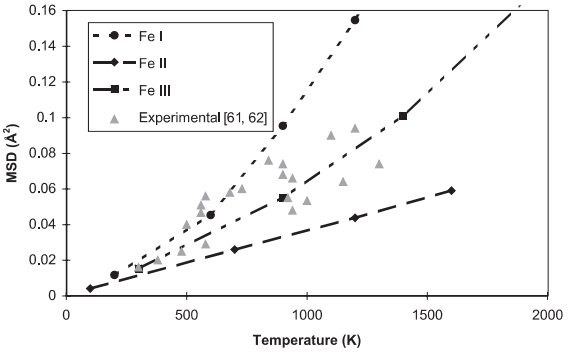

Fig. 2. Mean square displacements versus temperature for Fe I, Fe II and Fe III [61,62].

Table 5
Threshold displacement energies for α-Fe

PKA direction	E_d (eV)				
	Fe I	Fe II	Fe III	Finnis type potential[a]	Experimental[b]
⟨1 0 0⟩	19 ± 1	19 ± 1	17 ± 1	18 ± 1	17
⟨1 1 0⟩	51 ± 1	31 ± 1	47 ± 1	31 ± 1	>30
⟨1 1 1⟩	19 ± 1	19 ± 1	21 ± 1	>70	20

[a] Ref. [3]; [b] Ref. [46].

similar and close to the experimental results for all the potentials, although different procedures have been used. Note that the Finnis type potential gives a much too high value along the ⟨1 1 1⟩ direction.

3.2. FeCu

We dispose of three FeCu potentials, built from the three Fe potentials presented above (see Table 6 for details). We will just present below two important characteristics of these potentials.

When possible, a comparison is made with two other FeCu potentials found in literature

- a potential derived by Ackland et al. [34] from an Fe potential slightly different from the Finnis type potential;
- a potential derived by Osetsky et al. [41,50,51].

3.2.1. Partial molar energy of Cu at infinite dilution

For a regular solution, the mixing energy $\Delta E_m{}^c$ is given by $\Delta E_m^c = \Omega c(1-c)$ where Ω is an energy parameter (corresponding to the partial molar energy of the solute at infinite dilution or the heat of solution) and c is the solute concentration. Table 7 presents the values obtained for each potential at infinite dilution as well as the value obtained by Ackland et al. [34] for their FeCu potential. The experimental values are quite scattered, as they are computed from Cu solubility limits that are very scattered specially at low temperatures.

Table 6
Summary of the origins of the FeCu potentials investigated in this work

	Component	Equilibrium potential	Hardening
FeCu I	Fe I	Harrison[a]	Turbatte[b]
	Cu	Prönnecke[c]	Prönnecke[c]
	Cross	Becquart	Turbatte[b]
	FeCu		
FeCu II	Fe II	Haftel[d]	Vascon[e]
	Cu	Prönnecke[c]	Prönnecke[c]
	Cross	Becquart	Becquart
	FeCu		
FeCu III	Fe III	Simonelli[f]	Raulot[h]
	Cu	Voter[g]	Raulot[h]
	Cross	Ludwig[i]	Raulot[h]
	FeCu		
FeCu Ackland	Fe		
	Cu	Ackland[j]	Ackland[j]
	Cross		
	FeCu		

[a] Ref. [14]; [b] Ref. [15]; [c] Ref. [47]; [d] Ref. [17]; [e] Ref. [18,19]; [f] Ref. [20]; [g] Ref. [48]; [h] Ref. [21]; [i] Ref. [49]; [j] Ref. [34].

3.2.2. Threshold displacement energies for a Cu atom

The threshold displacement energies have been calculated when the recoil atom is a single substitutional copper atom and compared to those of pure Fe (values in parenthesis). The results are collected Table 8. Depending on the potentials, the threshold displacement energies of Cu in α-Fe can be different from those of Fe in α-Fe. Due to the lack of experimental data, it is difficult to assess the accuracy of these results.

More data about the FeCu potentials (Cu–Cu, Cu-vacancy binding energies compared to vacancy–vacancy binding energies, evolution of the lattice parameter versus Cu content, energy difference between bcc Cu and fcc Cu) can be found in a forthcoming paper dedicated more specifically to the study of the influence of Cu atoms on the displacement cascades [54].

4. Results

For the three potentials studied here, the overall damage picture is similar to what can be found in the literature, see for instance [55]: the cascade generates numerous defects; vacancies are mostly located near the core of the cascade while interstitials can be found mostly in the periphery. Some of the point defects formed are gathered in small clusters, others remain isolated. During the cascade event, replacement collision sequences (RCS) can be observed (Fig. 3). It has been recognized for some time now [1], that the primary state of damage is controlled at least by two phenomena: RCS during the ballistic phase as well as melting and resolidification during the relaxation and cooling phases [1]. RCS propagate at supersonic speed and are therefore able to transport interstitials beyond the core region before melting occurs. It has been observed many times that among the interstitials, mainly those that are transported beyond the melted core survive recombination. Big differences can be

Table 7
Partial molar energy of Cu at infinite dilution (heat of solution)

FeCu I (eV)	FeCu II (eV)	FeCu III (eV)	FeCu Ackland[a] (eV)	Experimental (eV)
0.57	0.312	0.497	0.317	0.317[a] 0.49[b] 0.59[c]

[a] Ref. [34]; [b] Ref. [52]; [c] Ref. [53].

Table 8
Threshold displacement energies for a Cu atom in an α-Fe matrix[a]

PKA direction	FeCu I (eV)	FeCu II (eV)	FeCu III (eV)	FeCu Ackland[b] (eV)
⟨1 0 0⟩	19 ± 1 (19 ± 1)	29 ± 1 (19 ± 1)	19 ± 1 (17 ± 1)	≈ 19 (≈ 20)
⟨1 1 0⟩	> 70 (51 ± 1)	> 60 (31 ± 1)	> 70 (47 ± 1)	> 100 (> 100)
⟨1 1 1⟩	19 ± 1 (19 ± 1)	21 ± 1 (19 ± 1)	19 ± 1 (21 ± 1)	≈ 32 (≈ 30)

[a] The values in parentheses are the threshold displacement energies for pure Fe.
[b] Ref. [34].

observed between the potentials, as potential FeCu II generates more and longer RCS than the others. This has a strong influence on damage generation and will be discussed in more details later on.

The exposure to radiation damage has been standardized and a usual way to characterize the radiation is the number of displaced atoms (DPA) predicted by the displacement model of Norgett–Robinson–Torrens (NRT) [56]. The DPA is correlated to the maximum number of Frenkel pairs created per atom in the materials. The NRT model predicts, for a PKA of given energy, the number of Frenkel pairs created to be $0.8E_{\mathrm{p}}/2E_{\mathrm{d}}$. E_{p} is the damage energy available for collisions and E_{d} is the average threshold displacement energy. The recommended value for α-Fe is 40 eV [57]. To a good approximation, E_{p} is the energy of the PKA in MD simulations. As is usually done, the results presented below are given relative to the NRT prediction.

4.1. Preliminary results 1: role of temperature

Temperature controls two different processes that are intimately related to the defect generation. The first is the thermal amplitude of the vibration of the atoms characterized by the MSD, the second is the diffusion of point defects which takes place at the end of the cascade essentially after the recombination phase. If the MSD is low, the atoms will remain close to their ideal lattice sites and the energy transmission from one atom to the next in the collision sequence will be more efficient. It will then be easier to have long RCS along dense directions of the lattice which are effective ways to produce residual defects. To assess the influence of the MSD, one should compare results obtained at the same reduced temperatures T/T_{m}. On the other hand, the absolute temperature will control the diffusion rate of the point defects once the lattice is thermalized. It has been observed that during the relaxation phases most of the recombination processes proceed athermally [3]; nevertheless, it is very likely that, during the cooling phase, the thermal diffusion processes will have some influence, specially in the formation of defect clusters.

As is usually done in literature, we compare results of displacement cascades obtained at the same absolute temperature, 600 K in most of the cases, as it is the pressure vessel steel temperature. When comparing, for a given potential, with some cascades done at 100 K, we found that a temperature increase (within this range) leads to slightly more defect creation at the cascade peak, and to slightly less residual defects in accordance with what is generally observed in MD simulations [9]. Stoller observed [58] that the temperature effect seems stronger at higher energies, but we do not have very high energy cascades ($E_{\mathrm{PKA}} > 30$ keV) to compare to his results.

4.2. Preliminary results 2: role of Cu

We have investigated the role of Cu atoms (these results will be published in a forthcoming paper [54]), and found that the small amount of copper atoms, considered here (0.2 at.%) does not seem to influence neither the number of defects created nor their spatial distribution. This fact and the lack of other groups' results for displacement cascades in FeCu are the reasons why, in a few cases, we compare our FeCu results to other groups' pure Fe results.

4.3. Shape of the cascade

The shape of the cascade is very important as the ratio 'volume to surface' will have an influence on the cooling rate of the damaged zone and on the amount of recombination and clusters' formation.

One obvious result is that the shape of the cascade is very much potential dependent. Fig. 3 presents typical

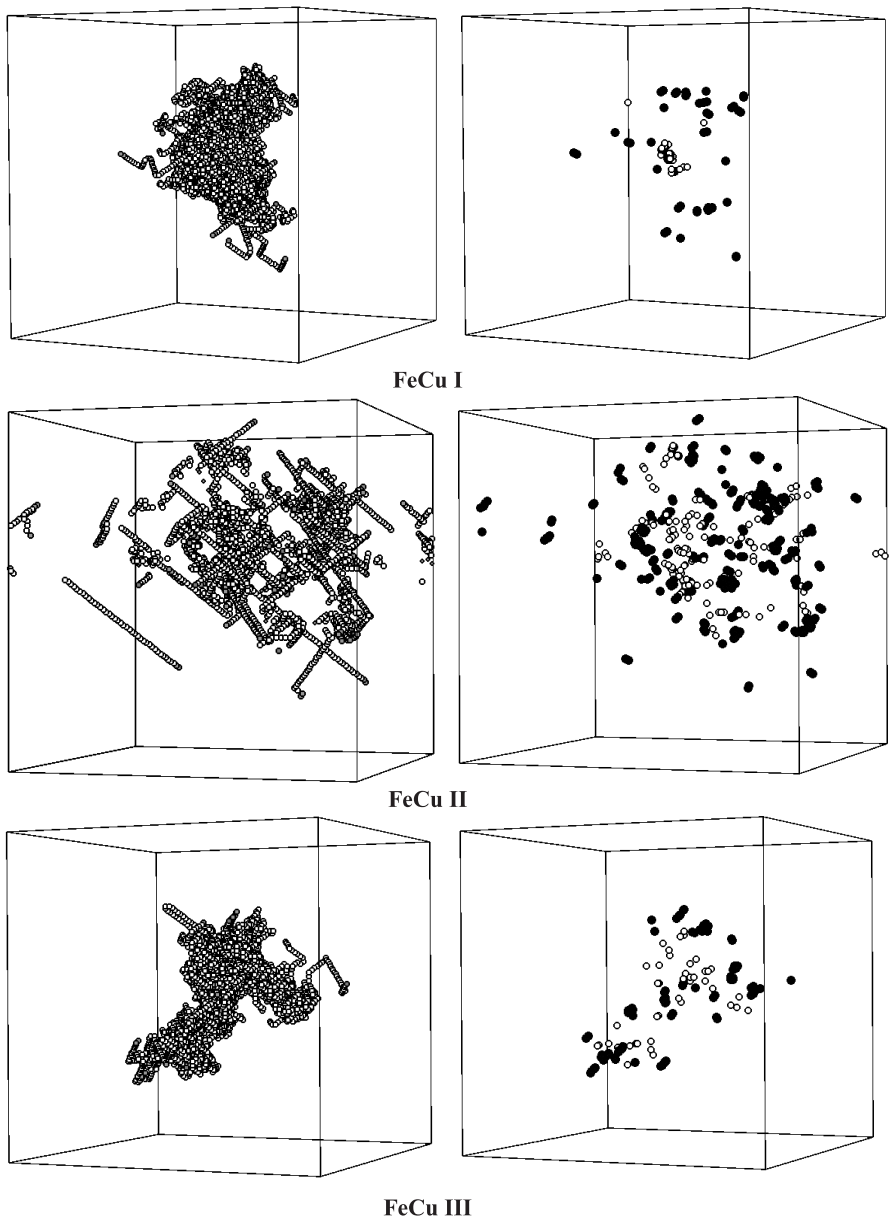

Fig. 3. Typical aspect of a 20 keV cascade at 600 K for the three FeCu potentials at the end of the recombination phase. Left-hand side: the empty circles are the replaced atoms, the dark circles are the interstitials. Right-hand side: the dark circles are interstitials, the empty ones are vacancies. Box size – 23 nm.

results of 20 keV cascades generated with the three potentials. It clearly appears that for FeCu III the shape is more isotropic and dense, while FeCu II give rise to a much less dense aspect with longer RCS. These general considerations remain unchanged whatever the energies and the temperatures we have investigated. Furthermore, the cascade shape differentiation appears clearly before the peak. One can also observe that the less dense the cascade, the more residual defects at the end: FeCu II leads to more numerous residual defects. These are, besides, located further away from the cascade core than the other two potentials defects.

4.4. Defect generation

The damage consists in two important components: the number of residual defects and their spatial distribution (tendency to form clusters, number and sizes of

the clusters). It has to be pointed out that these results are very much scattered as can be seen in Figs. 4 and 5. Even at high PKA energies, where one would expect the cascades to become more 'typical' and the fluctuations to become smaller, can large fluctuations be observed. For time and economical reasons it was not possible to obtain real statistics for each PKA energy, and only were the high energy cascades (10 and 20 keV) investigated more thoroughly to get an idea of the data scattering. To illustrate this point, the individual result of each cascade is represented instead of simulation averages.

4.4.1. Residual damage

The first important data one can extract from the simulations of displacement cascades is the residual damage which is left in the material once the cascade has cooled down. We call residual defects, the defects defined in 'computational procedure' which last more than 3 ps. We checked on a few cases that those defects do not disappear after 15 extra ps. The number of residual vacancies decreases when the PKA energy increases, for all potentials (Fig. 4) as is typically observed. However, it appears clearly that the potentials do not give the same results. FeCu II produces many more defects than the other two FeCu potentials which give closer results to the Finnis type potential for pure Fe (Fig. 4). This can be correlated with the cascade shape and will be discussed later on. It must be mentioned here, that we checked that the two defect characterization methods (ours and the Finnis type potential users) give similar results. The asymptotic value of the experimental defect efficiency (the number of residual vacancies relative to the NRT prediction) for α-Fe [55] is 0.39. This value is slightly higher than what can be deduced from Fig. 4 for all simulations but FeCu II which is obviously too high.

The number of replaced atoms at the end of the cascade gives additional and complementary information on the damage, as it is the number of atoms which have moved by at least one atomic spacing because of the cascade. In the case of alloys, it is a measure of the chemical mixing. The three potentials exhibit very different behaviors (Fig. 5). Like the residual vacancies amount, the number of replaced atoms can be correlated to the cascade shape.

The general trends that arise from the results is that the less dense the cascade (the more and the longer the RCS), the fewer the replaced atoms and the more the residual defects. This is illustrated Fig. 6 that clearly shows that the amount of recombination taking place during the relaxation and the cooling phases is also very much potential dependent.

4.4.2. Tendency to cluster and cluster size distribution

The tendency of the isolated defects created by the cascades to gather in clusters is a very important part of the damage picture one tries to obtain from the

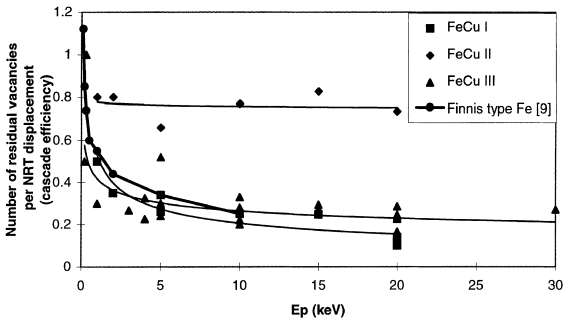

Fig. 4. Number of residual vacancies per NRT displacement (cascade efficiency) versus PKA energy at 600 K. The result of each cascade is represented instead of simulation averages. The drawn lines are only guidelines to show the trends.

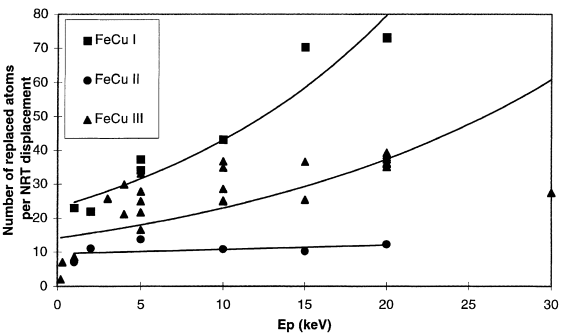

Fig. 5. Number of replaced atoms per NRT displacement versus PKA energy at the cascade's end at 600 K for FeCu I, FeCu II and FeCu III. To emphasize the scattering of the data, the result of each cascade is represented instead of simulation averages. The drawn lines are only guidelines to show the trends.

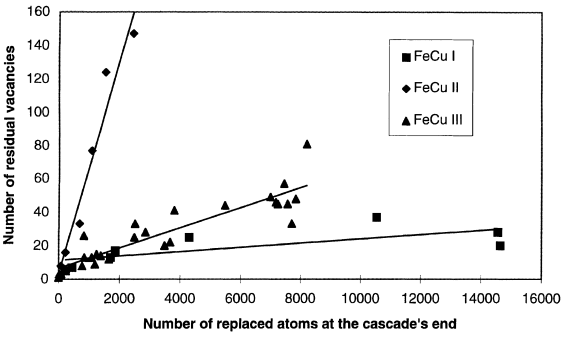

Fig. 6. Number of residual vacancies versus number of replaced atoms at the cascade's end at 600 K for FeCu I, FeCu II and FeCu III. The result of each cascade is represented instead of simulation averages. The drawn lines are only guidelines to show the trends.

simulations. Indeed it is well known that it strongly influences the later materials microstructure evolution.

Differences among the potentials can be noticed for the vacancy tendency to cluster and one potential (FeCu I) tends to form more vacancy clusters than the others (Fig. 7). There are no results available in the literature showing the tendency of vacancies to form clusters, except in the work of Stoller et al. [10]. This is probably due to the criterion used by the Finnis type potential group. Two vacancies have to be within nearest-neighbor distance to be considered belonging to the same cluster. It is therefore more restrictive a criterion than ours. To compare the clusters sizes obtained with the different potentials, the results are normalized by the number of clusters in each simulation. Potential FeCu I tends to form very big microvoids as can be seen Fig. 8, while the two other potentials behave similarly.

For the interstitials, the data scattering is very important and no real tendency appears (Fig. 9). The Finnis type potential [9] results do differ considerably by predicting a bigger tendency to cluster. Furthermore, a big difference between potential FeCu III and the other

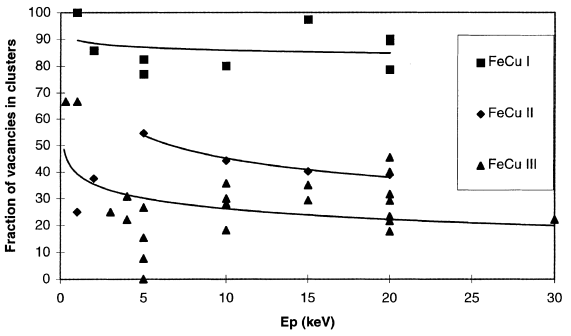

Fig. 7. Amount of vacancies in clusters versus PKA energy at 600 K for FeCu I, FeCu II and FeCu III. The result of each cascade is represented instead of simulation averages. The drawn lines are only guidelines to show the trends.

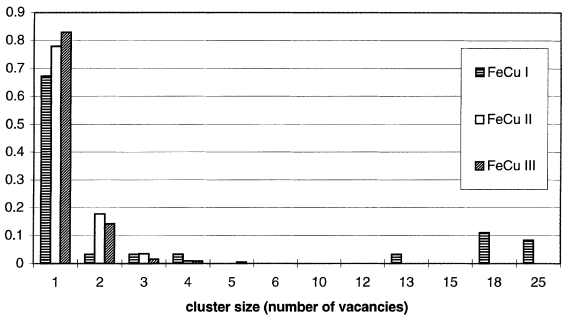

Fig. 8. Normalized vacancy cluster size distribution for 20 keV cascades at 600 K for FeCu I, FeCu II and FeCu III.

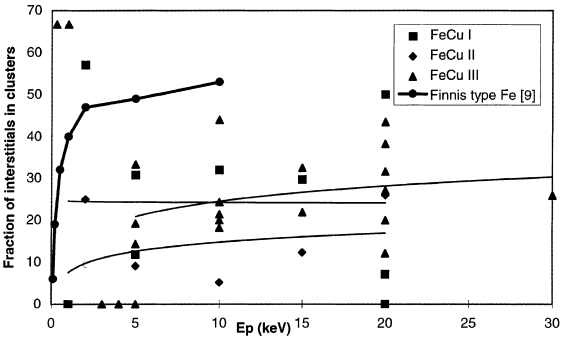

Fig. 9. Amount of interstitials in clusters versus PKA energy at 600 K for FeCu I, FeCu II, FeCu III and Finnis type Fe [9]. The result of each cascade is represented instead of simulation averages. The drawn lines are only guidelines to show the trends.

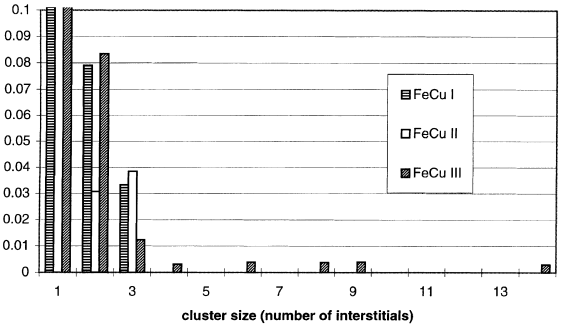

Fig. 10. Normalized interstitial cluster size distribution for 20 keV cascades at 600 K for FeCu I, FeCu II and FeCu III.

two potentials appears very clearly for 20 keV cascades. FeCu III form bigger interstitial clusters than the other two potentials (Fig. 10). Comparing our results to those of the group using the Finnis type potential, we only found, in the literature, the results of lower energy cascades: 5 and 10 keV. These 5 and 10 keV clusters are however bigger than our clusters at the same energies.

5. Discussion

We studied three different 'EAM-like' potentials which were fitted in the usual manner. These potentials however do not have the same characteristics: they lead to very different vacancy migration energies and defects formation energies; their thermal behaviors are also not alike and the results presented above show that when used for displacement cascade simulations, they lead to very dissimilar quantitative results. Even potential FeCu III, whose characteristics are very close to those of the Finnis type potential, gives rise to different results from

the latter for instance in the sizes of the interstitial clusters.

It now seems important to correlate these data with some characteristics of the potentials.

The cascades created with potential FeCu II exhibit long and numerous sequential replacement sequences and as a result they lead to the formation of many more residual defects than the other potentials (Fig. 4). The replacement sequences promote the formation of interstitial defects far away from the cascade core and thus decrease the probability of interstitial–vacancy recombinations. As the transmitted energy is focused along a few well determined directions, the cascades obtained are much less dense. A correlation can therefore be established between the cascade efficiency and its shape.

It is a natural assumption to suppose that the lower the MSD, the more and the longer the RCS, as explained above. Since potential FeCu II has very low MSD compared to the other potentials, we have made a couple of displacement cascades with a PKA energy of 10 keV at $T = 1050$ K. This temperature gives, for this potential, MSD equal to the experimental (and FeCu III) MSD at 600 K (see Fig. 2). The cascades shapes obtained at 1050 K are very similar to those obtained at 600 K. Also, there is no noticeable difference in the number of residual defects (taking into account the data scattering). Therefore, for potential FeCu II, in the 600–1050 K temperature range, the MSD influence on the RCS is not detectable. In other words, the propensity of this potential to form longer RCS at 600 K than the other potentials does not have a thermal origin. We have indications that this behavior is rather due to the repulsive part of the potential. At this point, it is worth recalling that the potentials have been hardened using different methods (for instance, the pair potentials of Fe II, Fe III and Finnis type potential have been spliced to the 'universal' screened-Coulomb potential of Biersack and coworkers [59] using different Born Mayer potentials) to give similar threshold displacement energies. This indicates thus, that having reasonable threshold displacement energies does not necessarily lead to a reasonable picture of the collision phase. It should, therefore, be interesting to find complementary data to fit to or to assess the validity of the potential hardening. Nevertheless, the influence of the MSD on the damage can be extracted when comparing results between potentials FeCu I and FeCu III. FeCu I which has high MSD leads to the formation of slightly less defects than FeCu III.

Two other important characteristics of the potentials which, we feel, are related to the tendency to form vacancy clusters are

- the easiness for a vacancy to move in the array, associated to (at thermal equilibrium) the vacancy migration energy $E_{\mathrm{vac}}^{\mathrm{m}}$;
- the tendency of a vacancy to bind with another vacancy or with a group of vacancies, characterized here by the vacancy–vacancy binding energy E_{VV}.

It is generally believed that the migration energies are not relevant in displacement cascades simulations because of the timescale involved (a few ps). However, a coincidence between the values of the migration energies and the tendency to form big vacancy clusters can be found (Table 2). Potential Fe I has a very low vacancy migration energy (0.1 eV) and tends to promote the formation of big vacancy clusters in the course of the displacement cascades. Potential Fe II has a very high migration energy (1.45 eV) and FeCu II forms small vacancy clusters while potential Fe III has a migration energy (0.66 eV) close to the experimental value (0.55 eV) and FeCu III exhibits an intermediate behavior. It is therefore likely that the vacancy migration energy or some aspect of the potential related to it like the roughness of the potential controls the mobility of vacancies even if they are not at thermal equilibrium.

The vacancy–vacancy binding energy is also important and potential Fe I does have a very high value for that energy. However, potential Fe III and the Finnis type potential have very similar vacancy–vacancy binding energies, and different vacancy migration energies, the Finnis type potential has a higher vacancy migration energy than potential FeCu III. To our knowledge, the displacement cascade simulations done with the Finnis type exhibit very little and small vacancy clusters. This may indicate that the vacancy migration energy is more important a parameter to control the tendency to form vacancy clusters than the vacancy–vacancy binding energy. Potential FeCu II which, like potential FeCu I, has a very high vacancy–vacancy binding energy also forms vacancy clusters. However, these are smaller, probably because of kinetics reasons. Because of a lack of data on the self interstitial binding energies and on the self interstitial migration energies, we cannot apply the same reasoning to the formation of self interstitial clusters but we believe that the results should be very similar. One, of course, should also take into account the fact that the mean distance between interstitials vary from one potential to another.

Other important parameters used in the literature to characterize the interatomic potentials are the defect formation energies. They vary sensibly from one potential to another and unfortunately no experimental data are available for the self interstitials formation energies. Adding up the energy needed to create a vacancy and the energy needed to create the most stable self interstitial defect for each potential gives a value of 8.21 eV for potential FeCu II, 5.17 eV for potential FeCu III, 4.73 eV for potential FeCu I and 5.74 eV Finnis type potential. Although these energies are very small compared to the cascade energies, and the cascade event far from the equilibrium conditions under which

Table 9
Summary of the cascades characteristics for the three potentials and their possible causes or the characteristics of the potentials it can be related to[a]

Cascades characteristics	Fe I	Fe II	Fe III	Possible causes or characteristics of the potentials
Amount of RCS	+	+++++	++	Short range interactions, MSD
DPA or number of replaced atoms	++++	+	++	MSD, $E_{\text{defects}}^{\text{formation}}$
Tendency to form vacancy clusters	++++	+(+)	++	$E_{\text{VV}}E_{\text{vac}}^{\text{m}}$
Number of residual defects	+	++++	++	easiness to recombine, MSD

[a] The number of + signs indicates the tendency: the more +, the higher the tendency.

they are determined, it appears that the values obtained are quite consistent with the number of defects created at the cascade peak. Similarly to the vacancy migration energy, the equilibrium defects formation energies may be correlated to the roughness of the potentials, and therefore give information about the processes taking place during the displacement cascades. Potential FeCu I has the lowest value and generates the most defects at the peak, while potential FeCu II exhibits a very high vacancy + interstitial formation energy and generates few defects at the peak. However, we are not able to establish a general correlation between the number of defects at the peak and the final damage.

It is interesting to recall here that none of our three potentials stabilize the correct type of dumbbell, and this, because of the range of the potential. We have mentioned previously that it seems that [20], in order to stabilize the right kind of self interstitial defect with EAM-like potentials, one must use very short range potentials (with a cut-off radius between the second and third nearest neighbor). We are not convinced of the importance or not of predicting the right kind of interstitial defect, however if the potentials are short ranged, then they give the same cohesive energy for the fcc and hcp structures (to be able to distinguish between the two structures, the potential range has to be at least longer than the fifth neighbor distance). We are not currently able to estimate the influence of this aspect on the estimate of the residual damage, but it is another point which emphasizes the need to use extreme care when trying to extract quantitative results from MD simulations.

In Table 9 we summarize our observations and the characteristics of the potentials we believe they can be related to.

6. Conclusions

We have investigated the influence of the interatomic potential on the residual damage by doing MD simulations of displacement cascades with one code and three different potentials published in literature. We found that the primary damage is very much potential sensitive. From our study, it appears that some characteristics of the potentials have a sensible influence on the results of cascade displacement simulations. Among these, the short range interactions (below the nearest-neighbor distance) seem to have a great effect and care should be taken concerning the hardening of a potential to study radiation damage. We feel that thermal properties also play an important role in the relaxation and cooling phases but this role is more subtle and needs further investigation. The vacancy migration energies and the vacancy–vacancy binding energies also appear to have some influence and should be investigated carefully in the radiation damage simulations.

Among the three potentials we have studied in this paper, potential Fe III appears to be the most adapted to the displacement cascades simulations because of its thermal behavior closer to the experimental one and the defect efficiency it predicts.

References

[1] T. Diaz de la Rubia, R.S. Averback, H. Hornming, R. Benedek, J. Mater. Res. 4 (1989) 579.
[2] K. Nordlund, R.S. Averback, Phys. Rev. B 56 (1997) 2421.
[3] A.F. Calder, D.J. Bacon, J. Nucl. Mater. 207 (1993) 25.
[4] A.J. Foreman, C.A. English, W.J. Phythian, Philos. Mag. A 66 (1992) 655.
[5] F. Gao, D.J. Bacon, Philos. Mag. A 71 (1995) 43.
[6] Z. Huilong, R.S. Averback, M. Natstasi, Philos. Mag. A 71 (1995) 735.
[7] H.F. Deng, D.J. Bacon, Phys. Rev. B 53 (1996) 11376.
[8] J.B. Gibson, A.N. Goland, M. Milgram, G.H. Vineyard, Phys. Rev. 120 (1960) 1229.
[9] W.J. Phythian, R.E. Stoller, A.J.E. Foreman, A.F. Calder, D.J. Bacon, J. Nucl. Mater. 223 (1995) 245.
[10] R.E. Stoller, G.R. Odette, B.D. Wirth, J. Nucl. Mater. 251 (1997) 49.

[11] F. Gao, D.J. Bacon, P.E.J. Flewitt, T.A. Lewis, J. Nucl. Mater. 249 (1997) 77.
[12] M.S. Daw, M.I. Baskes, Phys. Rev. Lett. 50 (1983) 1285.
[13] M.W. Finnis, J.E. Sinclair, Philos. Mag. A 50 (1984) 45.
[14] R.J. Harrison, A.F. Voter, S.P. Chen, in: V. Vitek, D.J. Srolovitz (Eds.), Atomistic Simulation of Materials – Beyond Pair Potentials, Plenum, New York, 1989, p. 219.
[15] J.C. Turbatte, master of science thesis, Université de Marne la vallée, 1995.
[16] S. Prönnecke, A. Caro, M. Victoria, T. Diaz de la Rubia, M.W. Guinan, J. Mater. Res. 6 (1991) 483.
[17] M.I. Haftel, T.D. Andreadis, J.V. Lill, J.M. Heridon, Phys. Rev. B 42 (1990) 11540.
[18] R. Vascon, N.V. Doan, Radiat. Eff. Def. Solids 141 (1996) 375.
[19] R. Vascon, doctoral thesis, Université Paris XI, 1997.
[20] G. Simonelli, R. Pasianot, E.J. Savino, Mater. Res. Soc. Symp. Proc. 291 (1993) 567.
[21] J.M. Raulot, master of science thesis, Université de Marne la vallée, 1998.
[22] C.S. Becquart, K.M. Decker, C. Domain, J. Ruste, Y. Souffez, J.C. Turbatte, J.C. Van Duysen, in: Proceedings of the Third International Conference on Computer Simulation of Radiation Effects in Solids (COSIRES 1996), Rad. Eff. Def. Solids 142 (1997) 9.
[23] A version in C-programming language is available at http://www.ims.uconn.edu/centers/simul/index.htm#xmd.
[24] J.R. Beeler, G.L. Kulcinski, in: P.C. Gehlen, J.R. Beeler, R.I. Jaffee (Eds.), Interatomic Potentials and Simulation of Lattice Defects, Plenum, New York, 1972, p. 735.
[25] C.H. Bennett, in: A.S. Norwick, J.J. Burton (Eds.), Diffusion in Solids, Recent Developments, Academic Press, New York, 1975, p. 85.
[26] C. Kittel, Introduction to Solid State Physics, 6th ed., Wiley, New York, 1987.
[27] J.A. Rayne, B.S. Chandrasekhar, Phys. Rev. B 122 (1961) 1714.
[28] B.N. Brockouse, H. Abou-Helal, E.D. Hallman, Solid State Commun. 5 (1967) 211.
[29] C.J. Smithells, Metals Reference Book, Butterwoths, London, 1967.
[30] A. Machova, G.J. Ackland, Model. Simul. Mater. Sci. Eng. 6 (1998) 521.
[31] L.D. Schepper, D. Segers, L. Dorikens-Vanpraet, M. Dorikens, G. Knuyt, L.M. Stals, P. Moser, Phys. Rev. B 27 (1983) 5257.
[32] H.E Schaefer, K. Maier, M. Weller, D. Herlach, A. Seeger, J. Diehl, Scripta Met. 11 (1977) 803.
[33] A. Vehanen, P. Hautojärvi, J. Johansson, J. Yli-Kauppila, P. Moser, Phys. Rev. B 25 (1982) 762.
[34] G.J. Ackland, D.J. Bacon, A.F. Calder, T. Harry, Philos. Mag. A 75 (1997) 713.
[35] C. Domain, unpublished results.
[36] K. Masuda, J. Phys. 43 (1982) 921.
[37] A. Weidinger, R. Wessner, T. Wichert, E. Recknagel, Phys. Lett. 72A (1979) 369.
[38] W. Chambron, J. Verdone, P. Moser, in: Conference on Fundamental Aspects of Radiation Damage in Metals, Gatlinburg, 1975, p. 261.
[39] H. Maeta, F. Ono, T.J. Kittaka, J. Phys. Soc. Japan 53 (1984) 4353.
[40] Yu.N. Osetsky, M. Victoria, A. Serra, S.I. Golubov, V. Priego, J. Nucl. Mater. 251 (1997) 34.
[41] Yu.N. Osetsky, A.G. Mikhin, A. Serra, J. Nucl. Mater. 212–215 (1994) 236.
[42] E.G. Moroni, G. Kresse, J. Hafner, J. Furthmüller, Phys. Rev. B 56 (1997) 15629.
[43] T. Kraft, M. Methfessel, M. van Schilfaarde, M. Scheffler, Phys. Rev. B 47 (1993) 9862.
[44] F.A. Lindemann, Physik. Z. 11 (1910) 609.
[45] J.J. Givalry, Phys. Rev. 102 (1956) 308.
[46] F. Maury, M. Biget, P. Vajda, A. Lucasson, P. Lucasson, Phys. Rev. B 14 (1976) 5303.
[47] S. Prönnecke, doctoral thesis, Lausanne, EPFL, 1992.
[48] A.F. Voter, Los Alamos unclassified Technical Report 93-3901, Los Alamos National Lab, 1993.
[49] M. Ludwig, D. Farkas, D. Pedraza, S. Schmauder, Model. Simul. Mater. Sci. Eng. 6 (1998) 19.
[50] Yu.N. Osetsky, A.G. Mikhin, A. Serra, Philos. Mag. A 72 (1995) 361.
[51] Yu.N. Osetsky, A. Serra, Philos. Mag. A 73 (1996) 249.
[52] R. Hultgren, P.D. Desai, D.T. Hawkins, M. Gleiser, K.K. Kelley, Selected Values of the Thermodynamic Properties of Binary Alloys, ASM, Metals Park, OH.
[53] M.H. Mathon, PhD thesis, CEA-5701, ISSN 0429-3460, 1995.
[54] C.S. Becquart, C. Domain, J.C. Van Duysen, in preparation.
[55] R.S. Averback, T. Diaz de la Rubia, Solid State Phys. 51 (1998) 281.
[56] M.J. Norgett, M.T. Robinson, I.M. Torrens, Nucl. Eng. Des. 33 (1975) 50.
[57] ASTM E693, Standard Practice for Characterizing Neutron Exposures in Ferritic Steels in Terms of Displacements per Atom (dpa), Annual Book of ASTM Standards, Vol. 12.02, American Society of Testing and Materials, Philadelphia, PA.
[58] R. Stoller, J. Nucl. Mater. 276 (2000) 12.
[59] J.P Biersack, J.F. Ziegler, Nucl. Instrum. Meth. 194 (1982) 93.
[60] G. Simmons, H. Wang, Single Crystal Elastic Constants and Calculated Aggregate Properties: A Handbook, MIT, Cambridge, 1971.
[61] C.W. Haworth, Philos. Mag. 5 (1960) 1229.
[62] P. Debrunner, R.J. Morisson, Rev. Mod. Phys. 36 (1964) 463.